Earthquake Geotechnical Engineering for Protection and Development of Environment and Constructions – Silvestri & Moraci (Eds)
© 2019 Associazione Geotecnica Italiana, Rome, Italy, ISBN 978-0-367-14328-2

Seismic induced landslides in sand: A numerical approach

A. Amorosi, F. Rollo & E. Lilliu
Department of Structural and Geotechnical Engineering, Sapienza University of Rome, Rome, Italy

ABSTRACT: In this paper we analyse numerically the behaviour of an ideal sandy slope subjected to an earthquake, aiming at exploring the possible triggering and propagation of instability conditions within the domain. At the scope an advanced constitutive model is adopted within a non-linear fully-coupled dynamic finite elements environment.

1 INTRODUCTION

Landslides are often triggered by seismic events (e.g.: Cetin et al 2004, Uzuoka et al 2005). The mechanism and evolution of such an instability problem is crucially influenced by the soil behaviour. In particular, coarse-grained soils can be characterised by the accumulation of significant shear strain and excess pore water pressures during the cyclic excitation induced by an intense earthquake, thus leading to a worse scenario in a potentially unstable slope as compared to that already induced in the slope by the inertial effects.

The numerical prediction of the response of this class of natural or artificial slopes subjected to seismic-induced dynamic actions is not trivial, as all the fundamental ingredients of the mechanics of sands should be accounted for. In fact, the constitutive assumptions should be capable to describe the accumulation of deformation, the degradation of the shear stiffness, the increase of damping and, finally, the build-up of the excess pore water pressures. Most of the single surface plasticity-based constitutive models proposed in the literature to mimic the monotonic response of sands are, generally, not able to capture the above essential features of their cyclic response. On the contrary, more advanced elasto-plastic constitutive models reveal to be more appropriate at this scope. Among them the so called Simple ANIsotropic SAND constitutive models (SANISAND), originally developed by Manzari & Dafalias (1997), have received much attention in the research community, as they explicitly account for some of the above-mentioned key features of the cyclic response of sands, including early irreversibility and the fundamental relationship between the dilatancy of the soil and its state, here described by a parameter expressed by the combination of the mean effective stress and the relative porosity of the material with respect to the critical state one (Been & Jeffries 1985). This latter ingredient plays a crucial role when modelling the flow liquefaction and the cyclic mobility of the soil during the seismic excitation (Li & Ming 2000).

In this paper we study the seismic performance of an ideal gentle slope of homogeneous loose Toyoura sand, excited by the horizontal component of a real earthquake accelerogram (Kocaeli 1999) applied at the base of the 51 m high 2D plane strain numerical model. The results of a representative numerical dynamic analysis are illustrated to highlight the transition between the initially stable condition and the unstable one as observed during the seismic excitation, focusing on the displacements and excess pore water pressures patterns of evolution. The stress-strain behaviour of the sand, as extracted at different depth in slope, is discussed in detail and related to the overall response of the soil body. The response of the slope is also compared to that of a corresponding soil column, under 1D conditions, to properly highlight the different attitude of the two numerical models towards flow liquefaction and seismic mobility.

2 IDEALISED PROBLEM UNDER STUDY

The two-dimensional geometrical model adopted in this study is characterized by 240 m length and maximum height equal to 51 m. The ideal slope extends for 80 m along the horizontal direction with an inclination of 8° with respect to this latter, as depicted in Figure 1.

The dynamic analyses are performed for vertically propagated shear waves in the time domain, employing the 2D Finite Element code PLAXIS 2D under plain strain conditions. In order to limit the dimension of the elements, according to the requirement that the element size must be smaller than about one/eighth of the wavelength associated with the maximum frequency component of the input wave, the numerical model is discretised in 759 15-node triangular elements with average size of 5.8 m.

The model is initialised under K_0-conditions (K_0 = 0.5) considering a horizontal ground surface and a deposit of 51m height with unit weight of volume γ = 20 KN/m^3. Then a static analysis is performed under drained conditions, in which a portion of the model is removed to reach the final configuration of the slope. In these pre-seismic static stages, the boundary conditions are the standard ones characterised by total fixities at the bottom of the model while on the vertical sides of the soil domain the horizontal displacements are null.

In the dynamic stages the acceleration time history recorded at the station Arcelik during the Kocaeli (1999) earthquake plotted in Figure 2 is adopted as input motion at the bottom of the model along the horizontal direction. The signal is characterised by a peak ground acceleration a_{max}= 0.25 g and filtered at a frequency of 5 Hz. Figure 2 also depicts the Fourier spectrum.

For the dynamic phases the bottom of the mesh is assumed as rigid, prescribed displacements are applied along the horizontal direction (i.e. x-axis) and free field boundary conditions are adopted for the vertical surfaces. The water level coincides with the slope profile and the soil is assumed saturated and isotropic in terms of hydraulic conductivity, with a value k = 10^{-4} m/s, typical of sands. The flow boundary conditions are closed at the bottom and on the vertical sides of the domain while the water flow is allowed at the ground level.

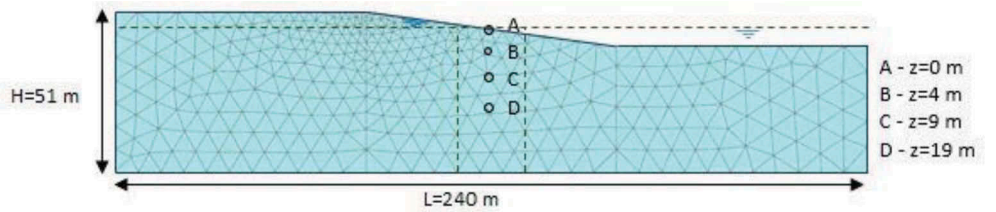

Figure 1. Geometry and discretisation of the numerical model

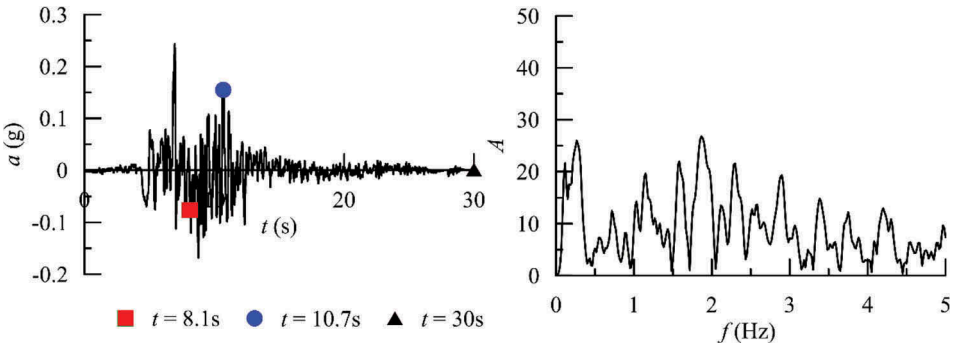

Figure 2. Acceleration time history and Fourier spectrum of the Kocaeli (1999) earthquake.

The dynamic analyses are performed using the option "dynamic analyses with consolidation" available in the code, in which the system of equations solves for acceleration, velocity, displacement and excess pore pressures simultaneously, following the *u-p* approach (Zienkiewicz et al. 1977). This technique simulates the coupling between soil deformations and transient seepage during the application of the acceleration time history, thus allowing for both accumulation and dissipation of excess pore pressures during the earthquake.

The standard Newmark solution scheme is adopted during the dynamic stages, with parameters $\alpha_N = 0.25$ and $\beta_N = 0.5$, ensuring the unconditional stability of the algorithm.

The proposed 2D numerical model is also adopted to perform an equivalent 1D analysis, considering the soil column depicted in Figure 1 subjected to the same input motion at the base. Comparing the 2D and 1D analyses highlights the role of the geometry-induced different states of the material and the related consequences on the cyclic response observed during the earthquake.

3 CONSTITUTIVE ASSUMPTIONS

In the following we adopt the Dafalias & Manzari (2004) model, which is based on bounding surface plasticity and critical state theory. Basically, the formulation includes four surfaces in the stress-ratio space. The yield surface is a cone with the apex at the origin of the stress space, capable of capturing the plastic response for variable stress ratios. The critical state surface is a cone with noncircular shape which controls the failure state of the material, characterised by shear deformations for fixed stresses and zero increments of volumetric strain. The material softening for dense states is governed by the bounding surface through the peak stress-ratio, while the dilatancy surface controls the plastic volumetric response during loading.

The state of the material is synthetically described by the state parameter $\Psi = e - e_c$, linking the effect of the current state of the material to the critical one, where e is the current void ratio and e_c is the corresponding critical void ratio at the current mean effective pressure (Been & Jefferies 1985). The bounding, dilatancy and critical surfaces are homothetic and function of Ψ. This latter dependence enables the simulation of the sand response with a single set of model parameters, irrespective of the initial conditions (i.e. loose or dense).

The model is characterised by a non-associated flow rule and by a kinematic hardening law that governs the evolution of the position of the yield surface with respect to the bounding one. For further details on the formulation of the model please refer to Dafalias & Manzari (2004).

In this study the loose Toyoura sand deposit, characterised by $e = 0.889$ corresponding to a relative density $D_r = 23.6\%$ is considered. The parameters of the model are those calibrated by Dafalias and Manzari (2004) based on drained and undrained triaxial compression tests (Verdugo & Ishihara 1996) (Table 1).

The initial states of the sand at points A-D of Figure 1 are represented in Figure 3 together with the projection of the critical state line. The soil is characterised by states denser than critical, with negative values of Ψ varying with the current mean effective pressure.

The assumed profile with depth of the elastic secant shear modulus G_{max} is plotted in Figure 4a while 4b-c illustrate the shear modulus decay curves and the variation of the damping ratio with shear strain, respectively. Those last curves were obtained performing a series of strain-controlled cyclic triaxial simulations under undrained conditions at initial void ratio $e_{in} = 0.889$. After an isotropic consolidation stage at a mean effective stress of 100 kPa, representative of the average stress level for the problem considered here, the ideal soil specimen was subjected to a vertical displacement varying with time by a sinusoidal law, so that its maximum value ranges from very small strain level (0.001 %) to relatively large one (0.1 %). At each investigated strain level the secant shear modulus and the damping ratio were evaluated with reference to the tenth cycle, recalling that the deviatoric strain is directly related to the shear strain γ by means of the relation $\gamma = \sqrt{3}\varepsilon_s$ (Georgiannou et al. 1991). In Figure 4c an additional damping $D = 1$ % is considered. In the dynamic analyses this quantity is introduced

Table 1. Summary of material constants of the SANI-SAND model for Toyoura sand.

Constant	Variable	Values
Elasticity	G_0	125
	ν	0.05
Critical state	M_c	1.25
	c	0.712
	λ_c	0.019
	e_0	0.934
	ξ	0.7
Yield surface	m	0.01
Plastic modulus	h_0	7.05
	c_h	0.968
	n^b	1.1
Dilatancy	A_0	0.704
	n^d	3.5
Fabric-dilatancy tensor	z_{max}	4
	c_z	600

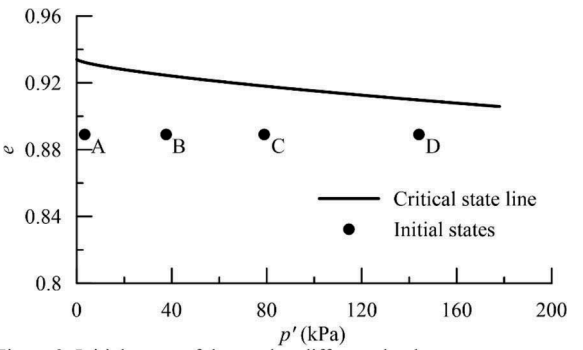

Figure 3. Initial states of the sand at different depths.

by the frequency-dependent viscous damping. Rayleigh coefficients are determined selecting the interval of frequencies as proposed by Amorosi et al. (2010).

The response of the model is characterised by the pronounced development of excess pore water pressure, leading to a rapid decrease of the mean effective stress and a consequent abrupt decrease of the secant shear modulus with increasing strain level. This feature represents a drawback of the model when simulating the behaviour of dense sands, which typically exhibit a smoother decay curve, as pointed out in Amorosi et al. (2018). However, for loose sands, as those under study, the original formulation of the model can realistically reproduce the development of excess pore water pressures under undrained conditions and satisfactorily interpret the cyclic mobility and liquefaction phenomena triggered during a seismic event.

The explicit integration of the Dafalias & Manzari (2004) model adopted in this work is that proposed by Mašín within the Soilmodel project (Gudehus et al 2008).

4 NUMERICAL RESULTS

The overall results of the fully coupled analysis are illustrated in Figure 5 in terms of contours of horizontal displacements u_x. The data are extracted at different times during the dynamic shaking, namely 8.1 s, 10.7 s and at the end of the signal (30 s), also indicated in Figure 2. The

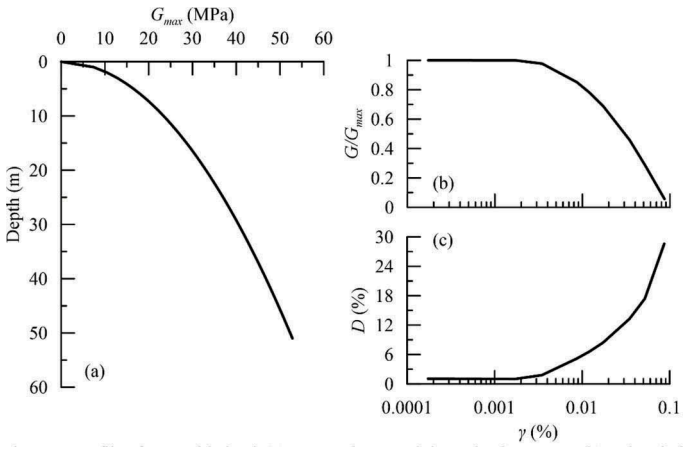

Figure 4. Profile of G_{max} with depth (a), secant shear modulus reduction curves (b) and variation of damping with shear strains (c).

slope begins to accumulate displacements slightly before the acceleration peak at about 7 s, already attaining about 0.5 m in its upper portion at t = 8.1 seconds. In the following 2.6 seconds the u_x at the same location increases up to about 1.3 m, while diffusing within the domain down to a depth of about 40 m.

At the end of the event the maximum cumulated horizontal displacements are about 2 m at the surface. Figure 5 also illustrates the cumulated horizontal displacements at the end of a different analysis, carried out under essentially drained conditions, assuming a very large

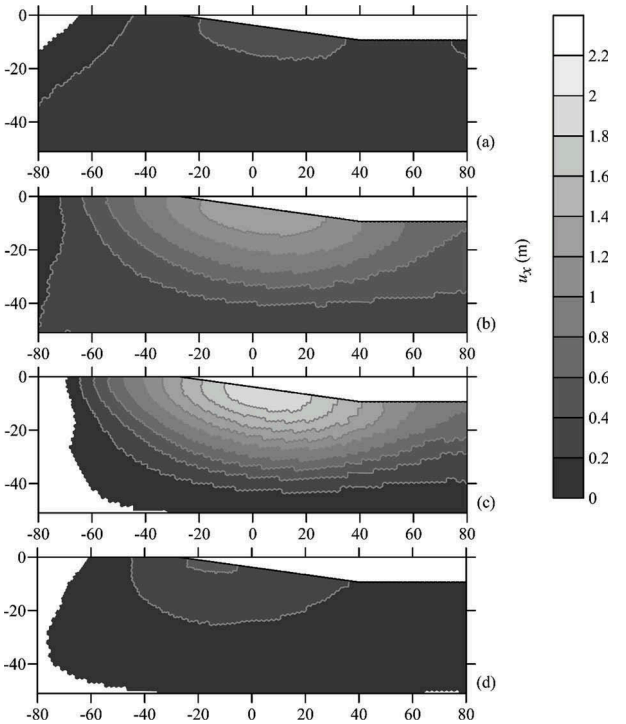

Figure 5. Horizontal displacements contour map at t = 8.1s (a), t = 10.7s (b), t = 30s (c) and at t = 30s for the drained analysis (d).

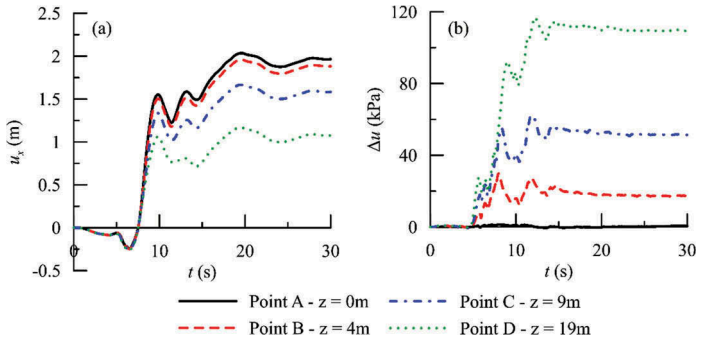

Figure 6. Horizontal displacements (a) and excess pore water pressure (b) for different depths.

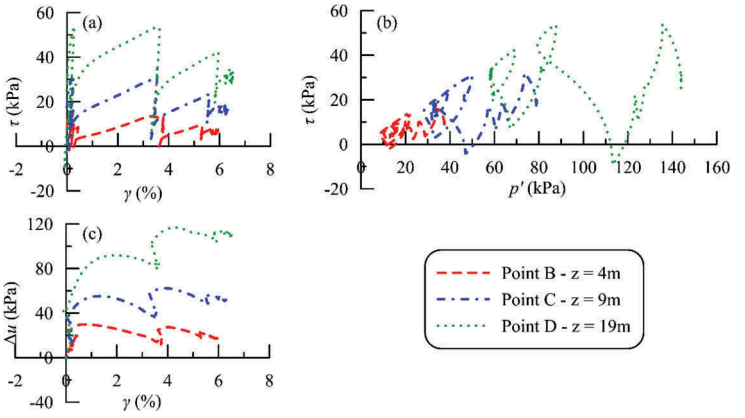

Figure 7. Stress strain curves (a), stress paths (b) and excess pore water pressure (c) for different depths.

hydraulic conductivity (k=1 m/s). In this case the accumulation of excess pore water pressure is prevented, and the cumulated displacements should only be ascribed to the inertial effects activated during the shaking, resulting in a much less deformed configuration of the slope.

Figure 6 shows the evolution of the horizontal displacement and excess pore water pressure with time for the nodes A-D indicated in Figure 1. Excess pore water pressure build up starts around t = 5.4 s, as a consequence of the first significant inversion of the acceleration which occurs slightly before (at t = 5 s) in the input signal of Figure 2. Positive horizontal displacements begin to accumulate with some delay with respect to the pore water pressures, with most of the process being concentrated in the first 10 s. In the remaining part of the analysis further displacement accumulation concentrates mainly in the upper portion of the domain.

To have an insight into the mechanics of the slope it is worth looking at the response of three Gauss points located in B, C and D (Figure 1), illustrated in Figure 7. The stress-strain curves plotted in the τ - γ plane are consistent with the overall displacement patters discussed above: after the initial relatively small strain amplitude cycles, all the points experience two major strain-accumulation stages, followed again by small strain cycles. For the more superficial points B and C most of the excess pore water pressure built up occurs before the large strain accumulation stages, while only at depth (point D) the process is extended throughout the whole straining of the material. Figure 7c shows the stress paths in terms of shear stress and mean effective pressure. At the beginning of the shaking all the investigated points are characterized by positive shear stresses. During the dynamic stage of the analysis they exhibit a similar pattern of behaviour: positive excess pore water accumulation induces a shift

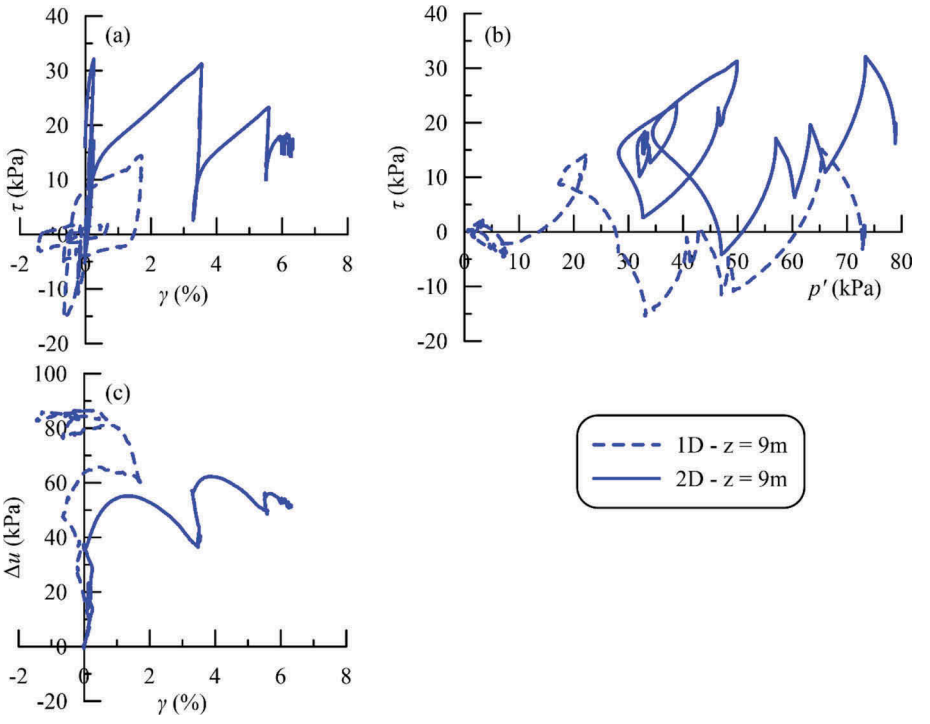

Figure 8. Stress strain curves (a), stress paths (b) and excess pore pressures (c) for 1D and 2D analyses.

towards lower values of p', while the crossing of the dilatancy line (i.e. phase transformation line in the Dafalias & Manzari model) triggers larger strain accumulation while stabilising the stress paths around fixed positive values of p'.

A reference equivalent 1D analysis was also carried for the soil column of Figure 1. Identical conditions characterise the two analyses, but for the slope-induced initial shearing. As such, the corresponding stress-strain behaviour observed at point C in the two analyses differs, as shown in Figure 8. The 1D scheme is more prone to flow liquefaction, as suggested by the continuous decrease of the mean effective stress towards the origin, where only residual stiffness and strength characterise the sand. On the contrary, the stress path of the 2D analysis stabilises at larger values of the effective stress, due to the cyclic mobility that emerges in relation to the partly dilatant response already discussed.

5 CONCLUSIONS

This paper studies a rather simple idealised slope of loose sand when subjected to a seismic event that temporarily induces unstable conditions within the soil mass. The fully coupled numerical approach, combined with the advanced constitutive assumptions here adopted, makes the results realistic enough to draw some conclusions:

- the inertial effect alone would not lead to the catastrophic outcomes of the analysis, which are critically triggered by the development of excess pore water pressures and its consequences on the stress paths experienced by the material;
- most of the large strains and related displacements observed during the shaking are cumulated while the soil exceeds the phase transformation line and approaches the critical state one, along a pattern often related to as cyclic mobility (Elgamal et al 2003);

- 1D scheme of analysis leads to a totally different pattern, where flow liquefaction prevails: in this case the stress path tends towards the origin leading to very low stiffness and strength;
- to capture the above features the adopted constitutive model should account for the state-dependency of its ingredients, including stiffness, flow rule and bounding surface (Li & Ming 2000).

REFERENCES

Amorosi, A., Boldini, D., & Elia, G. 2010. Parametric study on seismic ground response by finite element modelling. *Computers and Geotechnics*, *37*(4), 515–528.

Amorosi, A., Rollo, F., & Boldini, D. 2018. A modified bounding surface plasticity model for sand. In Numerical Methods in Geotechnical Engineering IX, Volume 1: *Proceedings of the 9th European Conference on Numerical Methods in* Geotechnical Engineering *(NUMGE* 2018), June 25-27, 2018, *Porto*, *Portugal* (p. 213). CRC Press.

Been, K., & Jefferies, M. G. 1985. A state parameter for sands. *Géotechnique*, 35(2), 99–112.

Cetin, K. O., Isik, N., & Unutmaz, B. 2004. Seismically induced landslide at Degirmendere Nose, Izmit Bay during Kocaeli (Izmit)-Turkey earthquake. *Soil Dynamics and Earthquake Engineering*, 24(3), 189–197.

Dafalias, Y. F. & Manzari, M. T. 2004. Simple plasticity sand model accounting for fabric change effects. *Journal of Engineering mechanics*, 130(6), 622–634.

Elgamal, A., Yang, Z., Parra, E., & Ragheb, A. 2003. Modeling of cyclic mobility in saturated cohesionless soils. *International Journal of Plasticity*, 19(6), 883–905.

Georgiannou, V.N., Rampello, S. & Silvestri, F. 1991. Static and dynamic measurements of undrained stiffness on natural overconsolidated clays. *10th European Conference on Soil Mechanics and Foundation Engineering, Firenze*, Vol. 1: 91–95.

Gudehus, G., Amorosi, A., Gens, A., Herle, I., Kolymbas, D., Mašín, D., ... & Tamagnini, C. 2008. The soilmodels. info project. *International Journal for Numerical and Analytical Methods in Geomechanics*, 32(12), 1571–1572.

Li, X. S., & Ming, H. Y. (2000). Unified modeling of flow liquefaction and cyclic mobility. *Soil dynamics and earthquake engineering*, 19(5), 363–369.

Manzari, M. T. & Dafalias, Y. F. 1997. A critical state two-surface plasticity model for sands. *Geotechnique*, 47(2), 255–272.

Uzuoka, R., Sento, N., Kazama, M., & Unno, T. 2005. Landslides during the earthquakes on May 26 and July 26, 2003 in Miyagi, Japan. *Soils and Foundations*, 45(4), 149–163.

Verdugo, R. & Ishihara, K. 1996. The steady state of sandy soils. *Soils and Foundations* 36(2): 81–91.

Zienkiewicz, O. C., Taylor, R. L., Zienkiewicz, O. C., & Taylor, R. L. 1977. *The finite element method* (Vol. 36). London: McGraw-hill.